Supporting Information

Stroud et al. 10.1073/pnas.1203193109

SI Materials and Methods

Estimating Relative Molecular Mass from Size Exclusion Chromatography. The mean relative molecular mass (M_r) of the toxic amyloid-β_{1-42} (Abeta42) fibrillar oligomer (TABFO) peak is estimated by interpolating the observed TABFO distribution coefficient (K_{av}) in the best-fit line of the observed K_{av} vs. the known $\log_{10}$ M_r for several commercially available protein standards (151–1901; Bio-Rad). The five molecular mass markers (gel filtration standard; Bio-Rad) used for the TABFO molecular mass calculation are vitamin B_{12} (M_r = 1,350), equine myoglobin (M_r = 17,000), chicken ovalbumin (M_r = 44,000), bovine γ-globulin (M_r = 158,000), and thyroglobulin (M_r = 670,000). The error of the estimate (σ_{Mr}) is propagated from the best-fit residual of the K_{av} measurements for the standard (σ_{KavS}) using the first-order Taylor series approximation (Eq. **S1**)

$$\sigma_{Mr} = 2.303 \cdot \sigma_{Kavs} \cdot 10^{(KavT-b)/m}, \quad \text{[S1]}$$

where K_{avT} is the measured K_{av} for TABFOs, b is the best-fit intercept with the K_{av} axis, and m is the slope of the best-fit line.

Sizing by Transmission EM. Particles are chosen by randomly selecting points on the image using a random number generator and then finding the closest particle to each of the random points. When two random points are very close to each other, the two closest particles to the two points are chosen. The shortest and longest dimensions of each selected particle are measured by counting pixels. For each particle, the M_r is estimated as a cylinder, with the M_r being (Eq. **S2**)

$$M_r = \frac{\pi \ell w^2}{4\rho}, \quad \text{[S2]}$$

where w is the width, ℓ the length, and ρ is the partial specific volume of 0.73 cm^3/g (1). In the cylinder approximation, we take the longest dimension as the length and the shortest dimension as the diameter for each particle. By our transmission EM (TEM) measurements, the TABFOs have a diameter of 7.0 ± 1.0 nm (SD; n = 50) and a length of 11 ± 2.0 nm (SD; n = 50). The error of the M_r is reported as the SEM for the 50 observations. The longest TABFO of our random sample is 15 nm. Although several oligomers much longer than 15 nm are visible in the micrograph in Fig. 1*C*, they represent just a small fraction of the visible particles and are excluded from the measurements by chance.

Size Estimate. The mean M_r of the oligomers is calculated from the combined measurements from TEM and size exclusion chromatography (SEC) by taking the average of the two measurements, with the error reported as the SEM for a sample of two observations (Eq. **S3**):

$$\sigma_A = \frac{|S-T|}{2}, \quad \text{[S3]}$$

where T and S are the TEM and SEC measurements, respectively.

Preparation of TEM Grids. Samples are added to glow-discharged 400 mesh carbon-formvar grids from Ted Pella (01754-F; Ted Pella). Staining is done with 1% (wt/vol) uranyl acetate. Samples are imaged with a FEI CM120 microscope at magnifications between ×19,000 and ×35,000.

Dot Blot Analysis. Five microliters each Abeta42 sample at the concentration of 1 mg/mL are spotted onto a nitrocellulose membrane (Trans-Blot; Bio-Rad). The membranes are blocked by 10% (wt/vol) fat-free milk in 50 mM Tris pH 7.4, 150 mM NaCl, and 0.05% (vol/vol) Tween20 (TBST buffer) for 1 h followed by incubation with antiamyloid fiber OC polyclonal antibody (~1:5,000 dilution) or Abeta 1–16 (6E10) monoclonal antibody (~1:2,500 dilution, SIG-39300; Covance) in 5% (wt/vol) fat-free milk and TBST buffer at room temperature for 1 h. Then, the membranes are washed three times in TBST buffer followed by incubating with anti-rabbit or anti-mouse antibody (1:5,000 dilution in 5% (wt/vol) fat-free milk and TBST buffer) at room temperature for 1 h. After the membranes are washed three times in TBST buffer, the films are developed with the Thermo Scientific Pierce ECL Western Blotting Substrate (32209).

Thioflavin T Fiber Assay. The thioflavin T (ThT) assay is performed on a Thermo-Scientific Varioskan Flash using top excitation and reading in sealed NUNC 96-well optical plates (265301; NUNC). Excitation and emission of ThT are performed at 440 and 484 nm, respectively. The time for fiber formation is measured as the time required for the signal to reach one-tenth of the maximum signal (tenth time).

FTIR Spectroscopy. FTIR spectra are taken on a JASCO FT/IR-420. A 200-μL aliquot containing 0.2 μg TABFOs is lyophilized and sandwiched between two 100-μg potassium bromide windows. The spectrum from the two windows alone is subtracted from the spectrum of the sandwich containing the lyophilized TABFOs. Linear baseline is applied to the spectrum. Deconvolution is performed as described in *Results* using in-house software written by J.C.S.

Cell Survival Assays. The MTT [3-(4,5-Dimethylthiazol-2-yl)-2,5-diphenyltetrazolium bromide] assay is performed using the CellTiter 96 nonradioactive cell proliferation assay kit (Promega). HeLa and PC-12 cells (CRL-1721; ATCC) are used to assess the toxicity of Abeta42 oligomers and fibers. Both PC-12 and HeLa cells are maintained at 37 °C in an atmosphere of 5% (vol/vol) carbon dioxide. PC-12 cells are cultured in ATCC-formulated RPMI medium 1640 (30–2001; ATCC) with 10% (vol/vol) heat-inactivated horse serum and 5% (vol/vol) FBS. HeLa cells are cultured in DMEM with 10% (vol/vol) FBS. Before treatment, PC-12 and HeLa cells are plated at 10,000 cells/well in 96-well plates (3596; Costar) and cultured for 20 h at 37 °C in an atmosphere of 5% (vol/vol) carbon dioxide; 10 μL sample are added to each well containing 90 μL medium. The plates are then incubated for 24 h at 37 °C in an atmosphere of 5% (vol/vol) carbon dioxide followed by adding 15 μL dye solution (G4000; Promega) for 4 h incubation at 37 °C in an atmosphere of 5% (vol/vol) carbon dioxide. Then, 100 μL solubilization Solution/Stop Mix (G4000; Promega) are added to each well. After incubation at room temperature for 12 h to fully solubilize the dye, the absorbance is measured at 570 nm (the background absorbance is recorded at 700 nm). SD is calculated from four replicates for each of the samples. The readout from the 0.05 M NH_4OH buffer-treated cell is taken as 100% survival, and the readout from the 0.2% SDS-treated cells is taken as 0% survival.

Circular Dichroism Spectroscopy. A JASCO J-715 spectrometer equipped with a JASCO PTC-348 temperature controller is used to acquire the circular dichroism spectra. Far UV spectra (240–195 nm) are collected in 0.1 cm path-length quartz cells. All measurements are conducted at 23 °C; 50 mM NH_4OH and PBS are used as blanks for subtraction from corresponding samples.

Fiber samples are in PBS buffer, and the Abeta oligomer sample is in 50 mM NH_4OH buffer.

X-Ray Powder Diffraction. Abeta42 samples are shot using copper radiation with 1.54 Å radiation from a rotating copper anode, and data are collected using a RAXIS-IV++ detector. Radial integration is performed using software written in-house by J.C.S. Images are divided into 100 resolution shells that are all equal in width as measured by $\sin(\theta)/\lambda$, where λ is the wavelength of the diffraction experiment and θ is the angle of diffraction. The radial integration is the average pixel value for each bin for all pixels above a background value. Averaged pixels also satisfy Chauvenet's criterion. For each image, the background value is found using the average pixel value from a corner of the image outside of the integration region. Using a background cutoff combined with outlier rejection reduces influence of the beam stop holder, discontinuity in CCD detectors, and spurious reflections that arise from salt crystals or other contaminants. Plots of the experimental data and scaled spectra (see below) are normalized such that the maximum over the range plotted is 1.0 and the background is 0.0 on the plot with linear stretching.

Modeling. Models are created using in-house software by J.C.S., and energy was minimized using CNS 1.2 (2). Protofilament models are created by stacking monomers as described in *Results*. Wrapping a protofilament around a helix entails three operations: shearing the protofilament, compressing the protofilament, and applying the helical transformation. The simplest case follows. If the direction of the helical axis is in Z and the shortest distance r from the protofilament axis to the helical axis is along Y, then shearing creates a second point (x', y', z') from the first point (x, y, z) (Eq. **S4**):

$$(x', y', z') = (x, y, z - x\tan\phi), \qquad \textbf{[S4]}$$

where ϕ is one-half of the crossing angle. Compression creates a third point (x'', y'', z'') (Eq. **S5**):

$$(x'', y'', z'') = (x'\cos\phi, y', z'\cos\phi). \qquad \textbf{[S5]}$$

Compression is needed, because the combination of shearing and applying the helical transformation stretches the wrapped object by sec ϕ (in X and Z for this example). Applying the helical transformation results in the fourth point (x''', y''', z''') (Eq. **S6**):

$$(x''', y''', z''') = \left(x''\cos\frac{z\tan\phi}{r}, y''\frac{z\tan\phi}{r}, z''\right). \qquad \textbf{[S6]}$$

This latter operation is equivalent to rotating the point (x'', y'', z'') around the helical axis by an angle $\theta = (z\ \tan\phi)/r$.

Using the present example and assuming that the protofilament is centered on the $Z = 0$ plane, we provide a description of the model with optimized β-sheet hydrogen bonding. To optimize β-sheet hydrogen bonding, the point (x''', y''', z''') is rotated backward around the helix axis and slid along Z. If the shortest distance between the point (x''', y''', z''') and the helix axis is r^*, then sliding along Z will make the fifth point (x^*, y^*, z^*) (Eq. **S7**):

$$(x^*, y^*, z^*) = \left(x''', y''', z'''\frac{\sqrt{\theta^2 r^2 + z'''^2}}{\sqrt{\theta^2 r^{*2} + z'''^2}}\right). \qquad \textbf{[S7]}$$

Rotating backward yields the final point (x^+, y^+, z^+) (Eq. **S8**):

$$(x^+, y^+, z^+) = (x''\cos)\sqrt{\frac{\phi^2 r^2 + z'''^2 - z^*}{r^{*2}}}, y''\sin\sqrt{\frac{\phi^2 r^2 + z'''^2 - z^*}{r^{*2}}}, z^*. \qquad \textbf{[S8]}$$

Domain swapping is achieved by redefining the connectivity of the monomers followed by molecular dynamics and energy minimization with CNS 1.2.

Two limitations affect the range of models that we test. First, the degree of wrapping or twisting influences the upper bound of the thickness, which we consequently limit to two protofilaments. Greater helicity results in the outermost sheets following longer paths than the innermost sheets, requiring lengthening of the β-hydrogen bonding of the outer sheets relative to the inner sheets. This distortion is greatly minimized but not eliminated in wrapping (3). Second, we limit the rotation between neighboring layers of the sheet (relative twist) to 2°–15°, corresponding to the range reported in previous studies of amyloid (4, 5). Although relative twist can be calculated for wrapping, we measure the degree of wrapping by the crossing angle of the two protofilaments (Fig. S2*D*). The crossing angle of a wrapped protofilament pair is measured by taking the tangents to the protofilament axes at the points where these axes intersect a line that is perpendicular to both. The crossing angle is formed by projecting the two tangents along the perpendicular line.

Scoring Simulated Powder Diffraction Patterns. Simulated patterns are XPREPX output with a Hanning smoothing function applied to simulate background scatter. Simulated patterns (C) are scaled to the experimental pattern (**T**) fitting the parameters α, β, and B to minimize the function (Eq. **S9**)

$$R^2 = \sum_j^N \left(\left\{\alpha\cdot\mathbf{C}_j\cdot e^{-2B\sin^2(\theta_j/\lambda)} + \beta\right\} - \mathbf{T}_j\right)^2, \qquad \textbf{[S9]}$$

where N is the number of bins, the subscript j indexes the bin, and θ_j is the bin center. This R^2 statistic is normalized to produce R_o^2, which we use to score the fit of the simulated powder diffraction patterns (Eq. **S10**):

$$R_0^2 = \frac{R^2}{\sum_j^N \left(\frac{\sum_k^N \mathbf{T}_k}{N} - \mathbf{T}_j\right)^2}. \qquad \textbf{[S10]}$$

1. Mok Y-F, Howlett GJ (2006) Sedimentation velocity analysis of amyloid oligomers and fibrils. *Methods Enzymol* 413:199–217.
2. Brunger AT (2007) Version 1.2 of the crystallography and NMR system. *Nat Protoc* 2: 2728–2733.
3. Wang J, Gülich S, Bradford C, Ramirez-Alvarado M, Regan L (2005) A twisted four-sheeted model for an amyloid fibril. *Structure* 13:1279–1288.
4. Jiménez JL, et al. (2002) The protofilament structure of insulin amyloid fibrils. *Proc Natl Acad Sci USA* 99:9196–9201.
5. Sunde M, et al. (1997) Common core structure of amyloid fibrils by synchrotron X-ray diffraction. *J Mol Biol* 273:729–739.

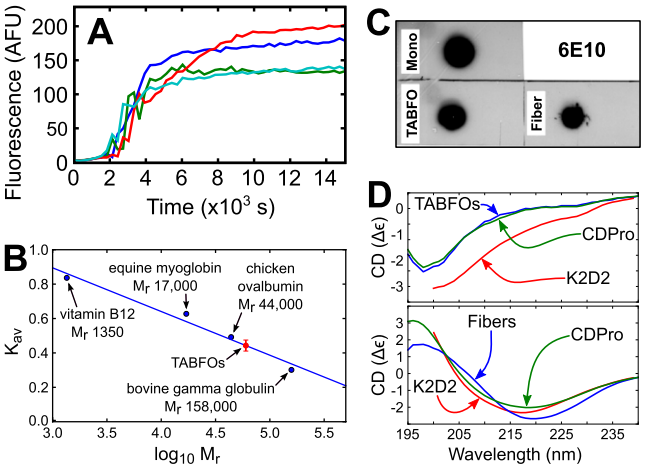

Fig. S1. TABFOs are β-rich fibrillar oligomers that are capable of fiber formation and about 20 Abeta42 monomers in size. (*A*) ThT fibrillogenesis assay shows that the Abeta42 that we prepare can serve as material for amyloid fibers. Four replicates from the same set of conditions (*Materials and Methods*) are shown in different colors. (*B*) Analysis of SEC shows that TABFOs have an M_r of 60,000 ± 4,200. SEC data shown in Fig. 1 are used for analysis. The observed distribution coefficient (K_{av}) is plotted against the known $\log_{10} M_r$ for the standards (blue). The K_{av} for TABFOs is plotted (red) against the interpolated TABFO M_r using the best-fit line to the standards (blue). The error bar on the TABFO point is the residual of the linear regression for the standards. This error in K_{av} is propagated to error in the estimate for the TABFO M_r as described in *SI Materials and Methods*. (*C*) Immunoblot with the Abeta-specific 6E10 antibody shows that differences in reactivity with the OC antibody (Fig. 2*A*) are not caused by loading differences. Fiber, Abeta42 fibers; Mono, Abeta42 monomers spotted immediately on resuspension into PBS after hexafluoroisopropanol (HFIP) treatment; TABFO, TABFOs prepared as described in *Results*. (*D*) Circular dichroism (CD) of TABFOs and fibers grown from TABFOs reveal that TABFOs have significant β-sheet structure. The fits from the K2D2 (1) and CDPro (2) software packages are shown. Secondary structure composition predictions from these programs are shown in Table 1. (*Upper*) Experimental CD spectrum of TABFOs. Blue, TABFOs; green, CDPro fit; red, K2D2 fit. (*Lower*) Experimental CD spectrum of fibers. Blue, fibers; green, CDPro fit; red, K2D2 fit.

1. Perez-Iratxeta C, Andrade-Navarro MA (2008) K2D2: Estimation of protein secondary structure from circular dichroism spectra. *BMC Struct Biol* 8:25.
2. Johnson WC (1999) Analyzing protein circular dichroism spectra for accurate secondary structures. *Proteins* 35:307–312.

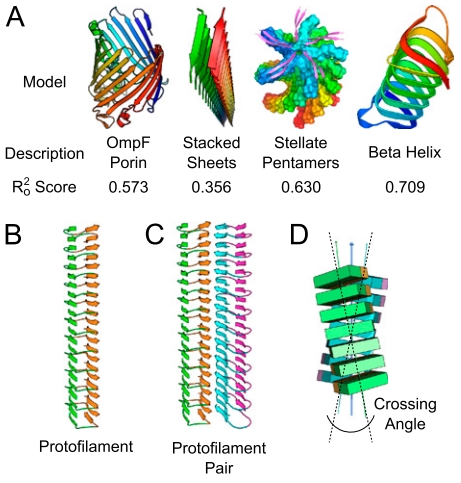

Fig. S2. Simulated powder diffraction patterns of models deviating from cross-β structure do not fit the TABFO experimental pattern as well as cross-β models composed of protofilaments. (*A*) Simulated powder diffraction pattern of β-barrels, stacked sheets, stellate oligomers, and β-helices are significantly different from the experimental powder diffraction pattern of TABFOs as measured by R_o^2. Cartoon representations of the models used for the simulated powder diffraction patterns in Fig. 3*B* with R_o^2 scores below. For clarity, the stellate pentamers are shown as one layer of cartoon atop seven layers of molecular surface representation. Antiparallel stacks of Abeta42 monomers are protofilaments that can be modeled as protofilament pairs with different geometries. (*B*) A protofilament is shown. The N-terminal strands of Abeta42 are green, and the C-terminal strands are orange. (*C*) The faces made by the C-terminal strands are on the interior of the protofilament pair. N-terminal strands are magenta or green. C-terminal strands are cyan or orange. (*D*) The crossing angle is measured by projecting the helical axes of these two protofilaments along a line of projection that is perpendicular to both axes. Tangents to the helical axes are taken at the points of intersection with the line of projection. When projected along the line of projection, the crossing angle is the angle between these two tangents. For our models, we allow the crossing angle to vary between 5° and 90°. The illustration looks down the line of projection, which is the perpendicular line.

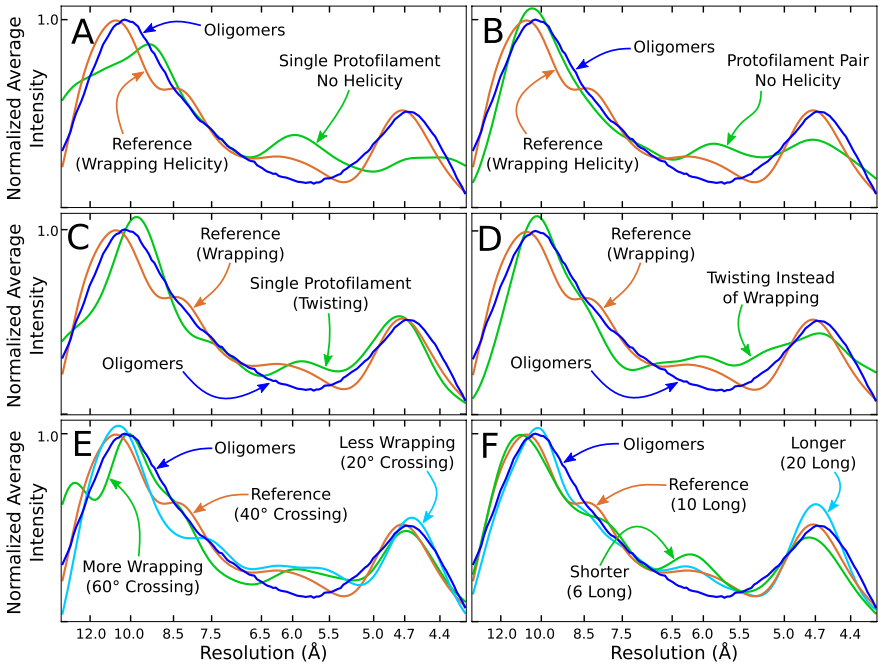

Fig. S3. Varying the model parameters shows that the simulated powder diffraction pattern from a wrapped protofilament pair fits the experimental pattern better than other types of models with cross-β structure. In all panels, the experimental pattern from TABFOs is shown in blue, and the reference pattern (40° crossing angle and 10 layers long) is shown in brown for comparison. Both the TABFO pattern and the reference pattern are the same as in Fig. 3. (*A*) The simulated powder diffraction pattern from the model of a single protofilament with no helicity (neither twisting nor wrapping) fits the general shape of the experimental pattern but does not match the peak shapes well. The simulated pattern from the 20-layer-long single protofilament model without helicity (R_o^2 = 0.290) is shown in green. (*B*) The pattern from a protofilament pair with no helicity fits the 10-Å peak well but lacks a well defined 4.7-Å peak. The simulated pattern from the 20-layer-long two-protofilament model with no helicity (R_o^2 = 0.135) is shown in green. (*C*) The pattern from a twisted single protofilament fits the 4.7-Å peak well, but the 10-Å peak is very sharp. The simulated pattern from the 20-layer-long twisted single protofilament (R_o^2 = 0.110) is shown in green. (*D*) The pattern from a twisted protofilament pair fits the 10-Å peak well but lacks a well-defined 4.7-Å peak. The simulated pattern from the 20-layer-long twisted protofilament pair (R_o^2 = 0.146) is shown in green. (*E*) The patterns from models with crossing angles between 30° and 70°, inclusively fit both peaks well. Models outside this range have less well-defined peaks, although the overall fit is good. The models here are 10 layers long, varying in the crossing angle. Cyan, 20° crossing angle; green, 60° crossing angle. These models are summarized in Table S1. (*F*) Varying the length of a wrapped protofilament pair does not significantly affect the fit of the simulated powder diffraction pattern to the experimental pattern. The models here have a 40° crossing angle but vary in length. Green, 6 layers long; cyan, 20 layers long. These models are summarized in Table S2.

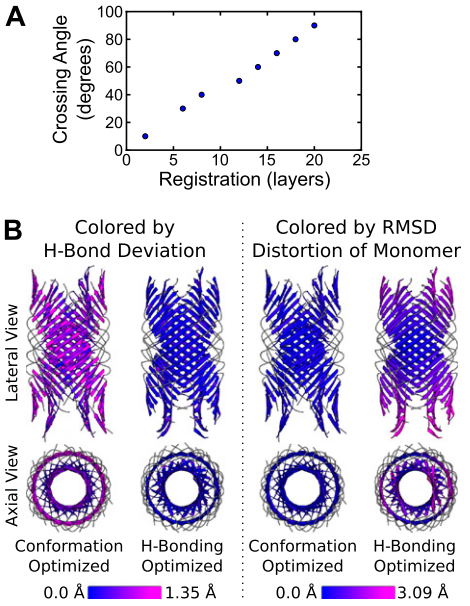

Fig. S4. Crossing angle is related to registration and deviation from ideal H-bond geometry. (*A*) Crossing angle increases as registration of the runaway domain swap increases. Various TABFO features, such as outside and hole diameters, are related to the registration. Several models were generated with varying crossing angles. The registration was determined for each model. (*B*) Tradeoff between optimal H-bonding and conformation for wrapped oligomers. Models that have a 70° crossing angle were generated. One model (right oligomer) has optimal β-sheet H-bond geometry enforced (see *SI Materials and Methods*). The other model (left oligomer) does not have optimal β-sheet H-bond geometry enforced. With H-bonding optimized, the end monomers undergo more distortion than the central monomers as the TABFO gets longer. When the conformation of the monomer is optimized (left oligomer), H-bonding undergoes more stretching at greater distances from the central axis, because the outermost sheets of a protofilament must wrap around a longer path than the innermost sheets. The longer path requires stretching the H-bonds in the outer sheets relative to the inner sheets. The TABFOs are shown as cartoon models with lateral views above axial views. The two TABFOs are colored by H-bonding deviation in *Left* and distortion of the monomer in *Right*.

Table S1. Crossing angle, hole diameter, and outside diameter of TABFO models increase with increasing registration of the runaway domain swap

Registration	Crossing angle (°)	Relative twist (°)	Length	R_o^2	Hole diameter (nm)	Outside diameter (nm)
2	10	2.05	10	0.167	<1	7.1
2	20	3.90	10	0.131	<1	7.3
6	30	6.08	10	0.086	<1	7.5
8	40	7.37	10	0.072	<1	8.0
14	60	8.96	10	0.130	1.4	8.2
16	70	9.05	10	0.093	2.0	8.6

Relative twist is the rotation between neighboring layers of the sheets (1). The fit to the experimental pattern (R_o^2) is robust to large variation in the registration. The hole and outside diameters are measured from axial projections of the TABFO models.

1. Sunde M, et al. (1997) Common core structure of amyloid fibrils by synchrotron X-ray diffraction. *J Mol Biol* 273:729–739.

Table S2. The fit to the experimental pattern (R_o^2) is robust to large variation in the length of the models

Length	R_o^2
6	0.117
10	0.072
12	0.071
14	0.063
20	0.052
30	0.058
50	0.061

The models are identical to the model in Fig. 3*C* except for the number of layers.

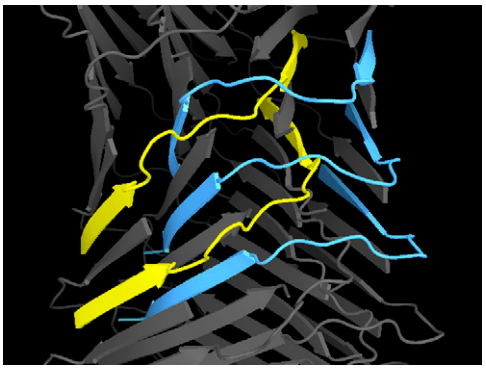

Movie S1. Overview of TABFO structure. The movie begins with the two runaway domain swaps colored cyan/yellow and magenta/green. Then, all monomers but one (cyan) fade to gray. The C-terminal partner of this first monomer fades in (yellow) followed by several monomers fading in; each is the C-terminal swapping partner of the previous monomer. The oligomer is then rotated around the superhelix axis 180° and then rotated for a view down the super helix axis.

Movie S1

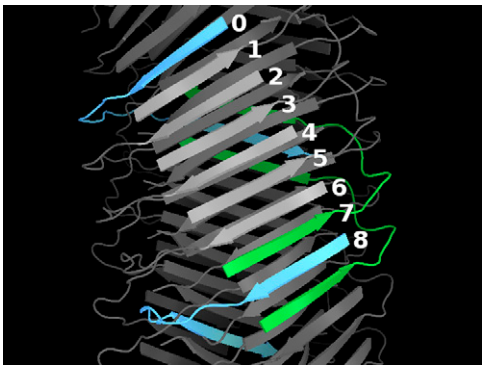

Movie S2. Measuring the registration of the runaway domain swap. The movie begins with the two runaway domain swaps colored cyan/yellow and magenta/green. Then, all monomers but one (cyan) fade to gray. This monomer (labeled 0) is followed to its C-terminal β-strand, which is part of the interior face for the green/cyan swap. This monomer's two neighbors in the β-sheet of the interior face fade in (green). These green monomers are followed to their N-terminal β-strands. The monomer that these N-terminal β-strands border fades in (cyan). The registration is then measured by counting the layer interfaces between this latter monomer and the monomer labeled 0. As gray strands take the number of the interface that they follow, they highlight for clarity. This TABFO model has a registration of eight.

Movie S2